

In J. Lellmann, M. Burger, J. Modersitzki (Eds.): Scale Space and Variational Methods. Lecture Notes in Computer Science, Vol. 11603, pp. 67–78, Springer, Cham, 2019. The final publication is available at link.springer.com.

Pseudodifferential Inpainting: The Missing Link between PDE- and RBF-Based Interpolation

Matthias Augustin, Joachim Weickert, and Sarah Andris

Mathematical Image Analysis Group, Faculty of Mathematics and Computer Science,
Campus E1.7, Saarland University, 66041 Saarbrücken, Germany
{[augustin](mailto:augustin@mia.uni-saarland.de),[weickert](mailto:weickert@mia.uni-saarland.de),[andris](mailto:andris@mia.uni-saarland.de)}@mia.uni-saarland.de

Abstract Inpainting with partial differential equations (PDEs) has been used successfully to reconstruct missing parts of an image, even for sparse data. On the other hand, sparse data interpolation is a rich field of its own with different methods such as scattered data interpolation with radial basis functions (RBFs).

The goal of this paper is to establish connections between inpainting with linear shift- and rotation-invariant differential operators and interpolation with radial basis functions. The bridge between these two worlds is built by generalising inpainting methods to handle pseudodifferential operators and by considering their Green’s functions. In this way, we find novel relations of various multiquadrics to pseudodifferential operators. Moreover, we show that many popular radial basis functions are related to processes from the diffusion and scale-space literature. We present a single numerical algorithm for all methods. It combines conjugate gradients with pseudodifferential operator evaluations in the Fourier domain. Our experiments show that the linear PDE- and the RBF-based communities have developed concepts of comparable quality.

Keywords: inpainting · sparse data · partial differential equations · pseudodifferential operators · scattered data interpolation · radial basis functions · Green’s functions.

1 Introduction

The problem of restoring damaged or lost parts of an image is known as inpainting. Solution strategies based on partial differential equations (PDEs) are very popular [22,2,26] since they can fill in missing (non-textured) data in a visually plausible way. This may even hold when the data become sparse. However, in this case one achieves best approximation quality if one optimises the inpainting data; see e.g. [1,21,13,6]. This idea is used successfully in inpainting-based

lossy image compression [12]. Although nonlinear anisotropic diffusion methods perform best in this application [12,24], linear operators such as homogeneous diffusion or biharmonic inpainting are often preferred: They are simpler and parameter-free, easier to analyse, and may give rise to faster algorithms [20,23].

Sparse inpainting can also be seen as a scattered data interpolation problem [11,29]. A popular approach in this field is the interpolation with radial basis functions (RBFs) [4]. Although these methods are most popular in geometric modelling and geosciences, they have also been used for image reconstruction; see e.g. [17,28,14]. However, to our knowledge, a systematic connection between linear PDE-based inpainting and scattered data interpolation cannot be found in the literature so far, and it is unclear how both paradigms perform in comparison.

Our Contribution. Our goal is to address these problems. We establish a general connection between inpainting with shift- and rotation-invariant PDEs and RBF-based interpolation. Since shift-invariant linear operators perform a pointwise multiplication in Fourier space, they are pseudodifferential operators. This motivates us to introduce the concept of pseudodifferential inpainting. By considering the Green’s functions of rotationally invariant pseudodifferential operators, we derive the desired link to RBFs. We identify popular RBFs with pseudodifferential operators that are diffusion and scale-space processes, and we evaluate the performance of pseudodifferential inpainting of sparse data.

Related Work. Pseudodifferential operators are not a novelty for researchers working on scale-spaces and variational methods. Already in 1988, Yuille and Grzywacz [30] have expressed Gaussian convolution as regularisation with a pseudodifferential operator. Pseudodifferential operators are also a natural concept for the class of α -scale-spaces (see e.g. Duits et al. [8]), which comprises the Poisson scale-space of Felsberg and Sommer [10]. Other scale-spaces that involve pseudodifferential operators and are relevant for our paper are the Bessel scale-spaces of Burgeth et al. [5]. More recently, Schmidt and Weickert [25] have introduced general shift-invariant linear scale-spaces in terms of pseudodifferential operators and identified their corresponding morphological evolutions. However, to the best of our knowledge, none of these pseudodifferential operators have been used in inpainting so far.

To solve harmonic and biharmonic inpainting problems, Hoffmann et al. [14] have used linear combinations of Green’s functions. Their considerations are our point of departure towards more general inpainting operators.

The connection between specific RBFs and partial differential operators, more precisely variational minimisation problems, was already used by Duchon [7] to establish thin-plate splines. Later on, several researchers derived suitable kernels for certain interpolation and approximation problems; see e.g. [16,19,9]. However, most publications are either specialised on one or two types of RBFs or consider the connection in a rather abstract setting. What is missing is a practical method that directly translates between an arbitrary (pseudo-)differential operator and a radial basis function. Our paper closes this gap.

Organisation of the Paper. In Section 2, we review the framework of harmonic inpainting and extend it to pseudodifferential inpainting. RBF inter-

polation is sketched in Section 3. We connect both worlds in Section 4 via the concept of Green's functions. Our numerical method, based on conjugate gradients and Fourier techniques, is described in Section 5, followed by a discussion of experimental results in Section 6. Section 7 gives a summary and an outlook.

2 From Harmonic to Pseudodifferential Inpainting

Let us consider a rectangular image domain $\Omega = [0, a] \times [0, b] \subset \mathbb{R}^2$ and a greyscale image $f: \Omega \rightarrow \mathbb{R}$, which is only known on a subdomain $K \subset \Omega$. A possible way to recover the missing data is so-called harmonic inpainting, which can be formulated as follows: Keep the data where it is known and solve the Laplace equation where no data is known, i.e.,

$$u = f \quad \text{on } K, \quad (1)$$

$$-\Delta u = 0 \quad \text{on } \Omega \setminus K, \quad (2)$$

with reflecting boundary conditions on $\partial\Omega$. This approach minimises the energy

$$E(u) = \int_K (u - f)^2 \, d\mathbf{x} + \int_{\Omega \setminus K} |\nabla u|^2 \, d\mathbf{x}, \quad (3)$$

where $|\cdot|$ denotes the Euclidean norm and ∇ the nabla operator in \mathbb{R}^2 .

We define the Fourier transform as

$$\widehat{u}(\boldsymbol{\zeta}) = \mathcal{F}[u](\boldsymbol{\zeta}) := \int_{\mathbb{R}^2} u(\mathbf{x}) \exp(-i 2\pi \boldsymbol{\zeta}^T \mathbf{x}) \, d\mathbf{x}. \quad (4)$$

The action of a linear, shift-, and rotation-invariant operator can be characterised by a factor $\widehat{p}(|\boldsymbol{\zeta}|)$ in the Fourier domain. This factor is called a *symbol*. Given a symbol, we can define a *pseudodifferential operator* $p(-\Delta)$ by reversing the Fourier transform, i.e.,

$$p(-\Delta) u(\mathbf{x}) := \int_{\mathbb{R}^2} \widehat{p}(|\boldsymbol{\zeta}|) \widehat{u}(\boldsymbol{\zeta}) \exp(i 2\pi \boldsymbol{\zeta}^T \mathbf{x}) \, d\boldsymbol{\zeta}. \quad (5)$$

For example, if we choose as operator the negative Laplacian $(-\Delta)$, its symbol is given by

$$\widehat{p}^{(-\Delta)}(\boldsymbol{\zeta}) = 4\pi^2 |\boldsymbol{\zeta}|^2. \quad (6)$$

This motivates the notation $p(-\Delta)$ for the pseudodifferential operators which we consider here.

An inpainting problem with a pseudodifferential operator reads

| | | |
|--------------------|---------------------------|-----|
| $u = f$ | on K , | (7) |
| $p(-\Delta) u = 0$ | on $\Omega \setminus K$, | (8) |

with reflecting boundary conditions.

Our pseudodifferential inpainting framework comprises naturally integer powers of the negative Laplacian. This so-called multiharmonic inpainting includes e.g. biharmonic and triharmonic inpainting. However, also non-integer powers $\alpha > 0$ are allowed, leading to α -harmonic inpainting. The special case $\alpha = 0.5$ yields Poisson inpainting. Also other pseudodifferential operators from scale-space theory can be used, for instance the Bessel operators. These and more examples of pseudodifferential operators and their symbols are listed in Table 1.

To interpret pseudodifferential inpainting in terms of energy minimisation, we allow only symbols which are nonnegative. Furthermore, we assume that the value zero is attained at most for $\zeta = \mathbf{0}$. Then the root of a pseudodifferential operator $p(-\Delta)$ is defined via

$$\sqrt{p(-\Delta)} u(\mathbf{x}) := \int_{\mathbb{R}^2} \sqrt{\widehat{p}(|\zeta|)} \widehat{u}(\zeta) \exp(i 2\pi \zeta^T \mathbf{x}) d\zeta, \quad (9)$$

and pseudodifferential inpainting minimises the energy functional

$$E(u) = \int_K (u - f)^2 d\mathbf{x} + \int_{\Omega \setminus K} \left(\sqrt{p(-\Delta)} u(\mathbf{x}) \right)^2 d\mathbf{x} \quad (10)$$

with reflecting boundary conditions. Table 1 also lists the corresponding penalising function

$$\Psi(u) := \left(\sqrt{p(-\Delta)} u(\mathbf{x}) \right)^2 \quad (11)$$

for each pseudodifferential operator.

Note that for a given pseudodifferential operator, the corresponding energy functional is not unique. For instance, for harmonic inpainting, Eq. (10) gives

$$E(u) = \int_K (u - f)^2 d\mathbf{x} + \int_{\Omega \setminus K} \left(\sqrt{-\Delta} u(\mathbf{x}) \right)^2 d\mathbf{x}, \quad (12)$$

which obviously differs from the energy functional (3). Here, the square root of the Laplacian $\sqrt{-\Delta}$ is the pseudodifferential operator defined by having $\sqrt{\widehat{p}(-\Delta)}(\zeta)$ as its symbol.

3 Interpolation with Radial Basis Functions

In the sparse interpolation problem we have in mind, K is a set of finitely many distinct pixels $\mathbf{x}_0, \dots, \mathbf{x}_N$ at which the image f is known. For RBF interpolation, the interpolating function u is obtained from the ansatz

$$u(\mathbf{x}) = \sum_{j=0}^N c_j g(|\mathbf{x} - \mathbf{x}_j|), \quad (13)$$

with a so-called *radial basis function* $g: \mathbb{R}_0^+ \rightarrow \mathbb{R}$. Popular choices include thin plate splines, polyharmonic splines, Matérn kernels, multiquadrics (MQs), inverse MQs, and inverse cubic MQs. Their formulas are displayed in Table 1.

The unknown coefficients $c_0, \dots, c_N \in \mathbb{R}$ are computed as solutions to the interpolation problem $u(\mathbf{x}_k) = f(\mathbf{x}_k)$ for all k . This yields the linear system

$$\sum_{j=0}^N c_j g(|\mathbf{x}_k - \mathbf{x}_j|) = f(\mathbf{x}_k) \quad \text{for all } k = 0, \dots, N. \quad (14)$$

A common condition to guarantee that this system has a unique solution is that its symmetric matrix $(g(|\mathbf{x}_k - \mathbf{x}_j|))_{j,k=0}^N$ is positive definite. Due to Bochner's theorem, this is equivalent to g having a positive (generalised) Fourier transform [29]. If the radial basis function has no compact support, the system matrix is dense. Then the numerical solution of the linear system is slow for large N .

Requiring a positive definite system matrix can be relaxed to positive semi-definiteness. For details and further information on RBF interpolation we refer to the monographs [4,29].

4 Connecting Both Worlds

Let us now establish a bridge between the pseudodifferential inpainting (8) and the RBF interpolation (13). Solving (8) requires inversion of a pseudodifferential operator, while (13) has a convolution-like structure. Thus, we employ the concept of *Green's functions*. The idea behind Green's functions is to define an inverse to a differential or pseudodifferential operator in the form of a convolution

$$(v \otimes g)(x, y) := \int_0^a \int_0^b v(s, t) g(x - s, y - t) dt ds. \quad (15)$$

A Green's function to the operator $p(-\Delta)$ is defined as a function g for which holds

$$p(-\Delta)(v \otimes g)(x) = v(x) \quad (16)$$

for all functions v which are orthogonal to the nullspace of $p(-\Delta)$ for all $\mathbf{x} \in \Omega$. Due to the convolution theorem, Fourier transform turns Eq. (16) into

$$\widehat{p}(|\zeta|) (\widehat{g}(|\zeta|) \widehat{v}(\zeta)) = \widehat{v}(\zeta) \quad \text{for all } \zeta \in \mathbb{R}^2. \quad (17)$$

At this point, the fact that v is orthogonal to the nullspace of $p(-\Delta)$ comes into play, as this means that $\widehat{v}(\zeta)$ equals zero whenever $\widehat{p}(|\zeta|)$ equals zero, such that Eq. (17) can still be satisfied in these cases. We can now obtain a Green's function g to $p(-\Delta)$ by defining its (generalised) Fourier transform to be

$$\widehat{g}(|\zeta|) := \begin{cases} 0, & \text{if } \widehat{p}(|\zeta|) = 0, \\ \frac{1}{\widehat{p}(|\zeta|)}, & \text{else,} \end{cases} \quad (18)$$

and the condition that g satisfies the reflecting boundary conditions on $\partial\Omega$. This shows that Green's functions are pseudoinverses to pseudodifferential operators.

We can also read Eq. (18) the other way around: Given a radial basis function $g(|\boldsymbol{x}|)$, compute its (generalised) Fourier transform $\widehat{g}(|\boldsymbol{\zeta}|)$ and use Eq. (18) to find the corresponding pseudodifferential operator $p(-\Delta)$ such that the chosen radial basis function is a Green's function to the newly defined pseudodifferential operator. Thus, Eq. (18) establishes a simple and elegant one-to-one mapping between pseudodifferential operators and radial basis functions. Consequently, pseudodifferential inpainting on sparse data is equivalent to sparse interpolation with radial basis functions.

Table 1 lists a number of pseudodifferential operators and their corresponding RBFs. For the sake of recognisability, we display the version of the functions which does not obey any boundary conditions. This is equivalent to considering a free-space problem, i.e., $\Omega = \mathbb{R}^2$. Moreover, the radial basis functions may differ from the Green's functions by a constant factor, which does not matter in applications.

Our results prove that many RBF concepts are equivalent to inpainting with well-known scale-space operators, ranging from α -scale-spaces to Bessel scale-spaces. Moreover, they also establish additional interesting findings, such as the interpretations of various MQs in terms of pseudodifferential operators.

One of the most important columns in Table 1 is the smoothness of the RBF, since (13) implies that it immediately carries over to the smoothness of the interpolant. On one hand, this column confirms some known facts such as the logarithmic singularity in the Green's function for harmonic inpainting, and the C^1 -smoothness of biharmonic inpainting. On the other hand, Table 1 displays also many smoothness results that are not well-known for the corresponding pseudodifferential operators. Note that all smoothness results hold only in 2D: For instance, the Green's function for harmonic inpainting is continuous with a kink in 1D, and it has a singularity of type $|\boldsymbol{x}|^{2-d}$ in \mathbb{R}^d for $d \geq 3$.

5 One Numerical Algorithm for All Approaches

Interestingly, our unifying framework for pseudodifferential inpainting also carries over to the discrete setting, where a single algorithm handles all approaches.

We replace the continuous image domain Ω by a regular Cartesian grid with n_x and n_y pixels in x - and y -direction. The corresponding grid sizes are h_x and h_y . Our discrete image is reflected in x - and y -direction to implement reflecting boundary conditions. The data on the resulting domain are then extended periodically such that we can apply the discrete Fourier transform.

We discretise the negative Laplacian by the usual five-point stencil with symbol

$$\widehat{p}_{\ell,m}^{(5)} = \left(\frac{2}{h_x} \sin\left(\frac{\ell\pi}{n_x}\right) \right)^2 + \left(\frac{2}{h_y} \sin\left(\frac{m\pi}{n_y}\right) \right)^2. \quad (19)$$

This ensures that Fourier and finite difference techniques produce identical results. To discretise other pseudodifferential operators, we substitute $4\pi^2 |\boldsymbol{\zeta}|^2$ in their symbol by $\widehat{p}_{\ell,m}^{(5)}$ and consider the results for all ℓ and m as eigenvalues of a

Table 1. Pseudodifferential operators, their symbols, radial basis functions along with their smoothness, and the penalising functions from (11). Negative signs are included where needed to obtain positive definite functions. Here, $t \in \mathbb{R}^+$, $[\cdot]$ is the floor function, K_ν is the modified Bessel function of the second kind of order $\nu \in \mathbb{R}$, ${}_2F_0(a, b; \emptyset; z)$ is a generalised hypergeometric function, and $\beta_n = \frac{2^{F_0(1,3-n;0;1)}}{(n-3)!}$.

| Operator $p(-\Delta)$ | Symbol \hat{p} | Radial Basis Function $g(\mathbf{x})$ | Smoothness of $g(\mathbf{x})$ | Penalising Function $\Psi(u)$ |
|---|--|---|---|--|
| $-\Delta$ harmonic [15] | $4\pi^2 \zeta ^2 =: \hat{p}(-\Delta)$ | singular harmonic spline [19] | $(\sqrt{-\Delta} u)^2$ | |
| $(-\Delta)^2$ biharmonic | $(\hat{p}(-\Delta))^2$ | $ \mathbf{x} ^2 \ln(\mathbf{x})$ thin plate spline [7] | C^1 | $(\Delta u)^2$ |
| $(-\Delta)^n$, $n \in \mathbb{N} \setminus \{1\}$ polyharmonic | $(\hat{p}(-\Delta))^n$ | $(-1)^n \mathbf{x} ^{2n-2} \ln(\mathbf{x})$ polyharmonic splines [29] | C^{2n-3} | $(\sqrt{-\Delta})^n u^2$ |
| $\sqrt{-\Delta}$ Poisson [10,3] | $\sqrt{\hat{p}(-\Delta)}$ | $ \mathbf{x} ^{-1}$ | singular | $(\sqrt[4]{-\Delta} u)^2$ |
| $(-\Delta)^\alpha$, $\alpha \in \mathbb{R}^+ \setminus \mathbb{N}$ α -harmonic [8] | $(\hat{p}(-\Delta))^\alpha$ | $(-1)^{[\alpha]} \mathbf{x} ^{2\alpha-2}$ α -harmonic splines [29,3] | singular for $\alpha \in (0, 1)$, $C^{2[\alpha]-2}$ for $\alpha > 1$, | $(\sqrt{-\Delta})^\alpha u^2$ |
| $(I - \frac{t}{\alpha} \Delta)^\alpha$, $\alpha \in \mathbb{R}^+$ Bessel [5] | $(1 + \frac{t}{\alpha} \hat{p}(-\Delta))^\alpha$ | $(\sqrt{\frac{\alpha}{t}} \mathbf{x})^{\alpha-1} K_{\alpha-1}(\sqrt{\frac{\alpha}{t}} \mathbf{x})$ Matérn kernels [27] | singular for $\alpha \leq 1$, $C^{2[\alpha]-2}$ for $\alpha \in (1, \infty) \setminus \mathbb{N}$ $C^{2\alpha-3}$ for $\alpha \in \{2, 3, \dots\}$ | $(\sqrt{(I - \frac{t}{\alpha} \Delta)^\alpha} u)^2$ |
| $\sum_{n=3}^{\infty} \beta_n t^n (\sqrt{-\Delta})^n$ | $\frac{(t\sqrt{\hat{p}(-\Delta)})^3 \exp(t\sqrt{\hat{p}(-\Delta)})}{1+t\sqrt{\hat{p}(-\Delta)}}$ | $-\sqrt{t^2 + \mathbf{x} ^2}$ multiquadric (MQ) [29] | C^∞ | $(\sqrt{\sum_{n=3}^{\infty} \beta_n t^n (\sqrt{-\Delta})^n} u)^2$ |
| $\sum_{n=0}^{\infty} \frac{t^n}{n!} (\sqrt{-\Delta})^{n+1}$ | $\sqrt{\hat{p}(-\Delta)} \exp(t\sqrt{\hat{p}(-\Delta)})$ | $t / \sqrt{t^2 + \mathbf{x} ^2}$ inverse MQ [29] | C^∞ | $(\sqrt{\sum_{n=0}^{\infty} \frac{t^n}{n!} (\sqrt{-\Delta})^{n+1}} u)^2$ |
| $\sum_{n=0}^{\infty} \frac{t^n}{n!} (\sqrt{-\Delta})^n$ | $\exp(t\sqrt{\hat{p}(-\Delta)})$ | $t / (t^2 + \mathbf{x} ^2)^{\frac{3}{2}}$ inverse cubic MQ [29] | C^∞ | $(\sqrt{\sum_{n=0}^{\infty} \frac{t^n}{n!} (\sqrt{-\Delta})^n} u)^2$ |



Figure 1. Test images *trui*, *peppers*, and *walter*.

matrix \mathbf{A} whose eigenvectors are given by the discrete Fourier transform. Then the discrete inpainting problem can be written as

$$\mathbf{C}(\mathbf{u} - \mathbf{f}) + (\mathbf{I} - \mathbf{C})\mathbf{A}\mathbf{u} = \mathbf{0}. \quad (20)$$

Here the vectors \mathbf{u} and \mathbf{f} are discretisations of u and f , and \mathbf{I} is the unit matrix. As \mathbf{C} has 1 on the diagonal for mask points and 0 for non-mask points, the first term in Eq. (20) corresponds to the interpolation condition (7), whereas the second term corresponds to Eq. (8). Rewriting (20) yields the linear system

$$(\mathbf{C} + (\mathbf{I} - \mathbf{C})\mathbf{A})\mathbf{u} = \mathbf{C}\mathbf{f}. \quad (21)$$

By considering only non-mask points, Eq. (21) can be reduced to a system of linear equations with a symmetric positive definite matrix with arguments similar to the ones in [20]. In other words, substituting some rows of a positive (semi)definite matrix \mathbf{A} by corresponding rows of a unit matrix yields a positive definite matrix. Thus, we can use a standard conjugate gradient (CG) solver. Its matrix–vector products with the circulant matrix $\mathbf{A} \in \mathbb{R}^{2n_x n_y \times 2n_x n_y}$ are computed in the Fourier domain with an effort that does not depend on the pseudodifferential operator. We stop the CG iterations when the Euclidean norm of the residual vector has dropped by a factor 10^{-20} .

6 Experiments

To evaluate the performance of the different pseudodifferential operators, we inpaint three greyscale images with size 256×256 and range $[0, 255]$: *trui*, *peppers*, and *walter* (Fig. 1). As known data, we use the grey values of each image at the locations given by a fixed random mask (Fig. 2 top left). Its density is 5%, i.e. we know the grey values for 5% of the pixels. The parameters α and t have been optimised by a simple grid search to produce the minimal mean squared error (MSE) w.r.t. the ground truth. Table 2 reports these errors for all three images, and Fig. 2 illustrates the inpainting results for *trui*.

We observe that Poisson inpainting performs much worse than all other approaches. It suffers from the strongly visible singularity of the RBF. The second worst is harmonic inpainting, whose logarithmic singularity is also visible.

Biharmonic, α -harmonic, MQ and inverse MQ inpainting produce very good results of comparable quality. For optimal parameters, their RBFs are at least in the smoothness class C^1 such that no singularities are visible. However, since these operators involve higher order powers of the Laplacian, they may violate a maximum-minimum principle. This becomes visible in over- and undershoots and ripple artifacts. These artifacts are slightly more pronounced for inverse cubic MQs, which is also confirmed by a somewhat worse MSE.

Bessel inpainting uses almost the same optimal α values as optimised α -harmonic inpainting, and its optimal t -values are large. In this setting both approaches are almost identical, since for large t , we have $(I - \frac{t}{\alpha}\Delta)^\alpha \approx (-\frac{t}{\alpha}\Delta)^\alpha$, and the latter is equivalent to α -harmonic inpainting.

The optimal α parameters for α -harmonic inpainting are close to 2. Thus, practitioners may prefer the parameter-free biharmonic inpainting as a method of choice. Since the corresponding thin plate splines can be seen as a rotationally invariant 2D extension of cubic spline interpolation, this also confirms earlier findings where cubic splines are reported as favourable interpolation methods [18]. Moreover, this indicates that on average, natural images can be approximated well by continuously differentiable functions.

The fact that biharmonic inpainting and the various MQs give results of similar quality is remarkable: It shows that the linear PDE community and the RBF community have reached a comparable level of maturity and sophistication, even without many interactions. Of course, for PDE-based inpainting, nonlinear methods may offer further improvements [12,24]. However, they cannot be treated adequately within a pseudodifferential framework, which is based on intrinsically linear concepts such as Fourier techniques.

Table 2. MSE results for the different inpainting approaches applied to the test images.

| Operator | <i>trui</i> | <i>peppers</i> | <i>walter</i> |
|--------------------|--|---|---|
| harmonic | 211.14 | 226.39 | 233.40 |
| biharmonic | 136.65 | 152.91 | 121.58 |
| Poisson | 759.26 | 751.61 | 773.27 |
| α -harmonic | 135.89 ($\alpha = 1.86$) | 152.57 ($\alpha = 1.9$) | 121.28 ($\alpha = 2.09$) |
| Bessel | 135.79 ($\alpha = 1.89, t = 485$) | 152.57 ($\alpha = 1.9, t = 10^6$) | 121.23 ($\alpha = 2.13, t = 386$) |
| multiquadric (MQ) | 137.97 ($t = 5.13$) | 166.83 ($t = 4.98$) | 124.34 ($t = 5.9$) |
| inverse MQ | 135.63 ($t = 3.89$) | 161.99 ($t = 3.79$) | 121.97 ($t = 4.63$) |
| inverse cubic MQ | 167.08 ($t = 7.05$) | 198.23 ($t = 6.79$) | 137.90 ($t = 7.11$) |

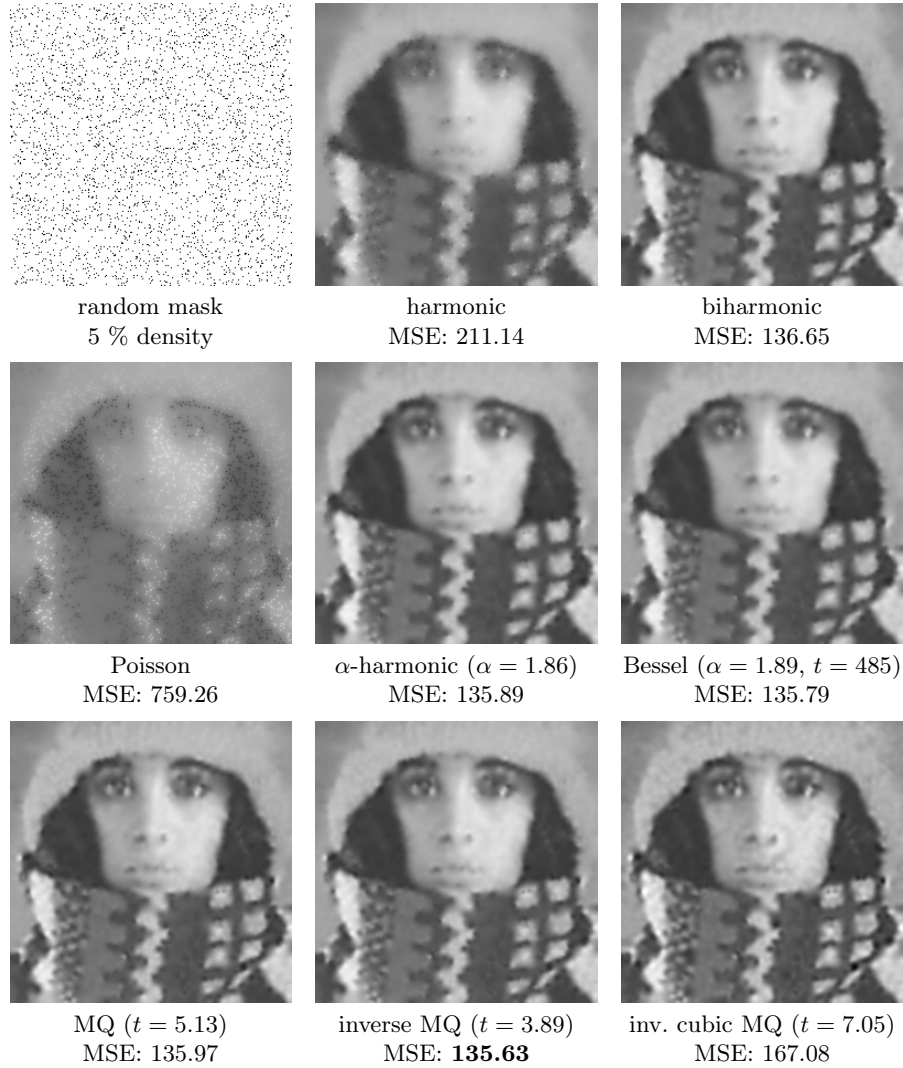


Figure 2. Inpainting results for the image *trui* from Fig. 1.

7 Conclusions and Outlook

We have established pseudodifferential inpainting as a unifying concept that connects linear PDE-based inpainting and RBF interpolation. This framework is surprisingly simple and general: It can handle any linear shift- and rotation-invariant operator, not only analytically but also algorithmically. It enabled us to find a number of interesting, hitherto unknown insights and relations, ranging from smoothness results for all inpainting methods to connections between RBFs and scale-space operators. Last but not least, we have shown that the linear PDE-

and RBF-based communities have come up with approaches of similar maturity and quality.

Currently we are investigating additional RBFs such as truncated RBFs, and we are going to extend our evaluation to the setting of inpainting-based compression. The latter involves several new aspects, e.g. their performance for optimised data and sensitivity w.r.t. quantisation.

Acknowledgement. This project has received funding from the European Research Council (ERC) under the European Union’s Horizon 2020 research and innovation programme (grant agreement no. 741215, ERC Advanced Grant IN-COVID).

References

1. Belhachmi, Z., Bucur, D., Burgeth, B., Weickert, J.: How to choose interpolation data in images. *SIAM Journal on Applied Mathematics* **70**(1), 333–352 (2009)
2. Bertalmío, M., Sapiro, G., Caselles, V., Ballester, C.: Image inpainting. In: Proc. SIGGRAPH 2000. pp. 417–424. New Orleans, LA (Jul 2000)
3. Bucur, C.: Some observation on the Green function for the ball in the fractional Laplacian framework. *Communications on Pure & Applied Analysis* **15**(2), 657–699 (2016)
4. Buhmann, M.D.: *Radial Basis Functions: Theory and Implementations*. Cambridge University Press, Cambridge, UK (2003)
5. Burgeth, B., Didas, S., Weickert, J.: The Bessel scale-space. In: Olsen, O.F., Florack, L., Kuijper, A. (eds.) *Deep Structure, Singularities, and Computer Vision*, Lecture Notes in Computer Science, vol. 3753, pp. 84–95. Springer, Berlin (2005)
6. Chen, Y., Ranftl, R., Pock, T.: A bi-level view of inpainting-based image compression. In: Kúkelová, Z., Heller, J. (eds.) *Proc. 19th Computer Vision Winter Workshop*. pp. 19–26. Křtiny, Czech Republic (Feb 2014)
7. Duchon, J.: Interpolation des fonctions de deux variable suivant le principe de la flexion des plaques minces. *Revue française d’automatique, informatique, recherche opérationnelle. Analyse numérique* **10**(12), 5–12 (Dec 1976)
8. Duits, R., Florack, L., de Graaf, J., ter Haar Romeny, B.: On the axioms of scale space theory. *Journal of Mathematical Imaging and Vision* **20**(3), 267–298 (2004)
9. Fasshauer, G.E., Ye, Q.: Reproducing kernels of generalized Sobolev spaces via a Green function approach with distributional operators. *Numerische Mathematik* **119**(3), 585–611 (Nov 2011)
10. Felsberg, M., Sommer, G.: The monogenic scale-space: a unifying approach to phase-based image processing in scale-space. *Journal of Mathematical Imaging and Vision* **21**(1), 5–26 (Jul 2004)
11. Franke, R., Nielson, G.M.: Scattered data interpolation and applications: A tutorial and survey. In: Hagen, H., Roller, D. (eds.) *Geometric Modeling: Methods and Applications*, pp. 131–160. Springer, Berlin (1991)
12. Galić, I., Weickert, J., Welk, M., Bruhn, A., Belyaev, A., Seidel, H.: Image compression with anisotropic diffusion. *Journal of Mathematical Imaging and Vision* **31**(2–3), 255–269 (Jul 2008)

13. Hoeltgen, L., Setzer, S., Weickert, J.: An optimal control approach to find sparse data for Laplace interpolation. In: Heyden, A., Kahl, F., Olsson, C., Oskarsson, M., Tai, X. (eds.) *Energy Minimization Methods in Computer Vision and Pattern Recognition*, Lecture Notes in Computer Science, vol. 8081, pp. 151–164. Springer, Berlin (Aug 2013)
14. Hoffmann, S., Plonka, G., Weickert, J.: Discrete Green’s functions for harmonic and biharmonic inpainting with sparse atoms. In: Tai, X.C., Bae, E., Chan, T.F., Lysaker, M. (eds.) *Energy Minimization Methods in Computer Vision and Pattern Recognition – EMMCVPR 2015*, pp. 169–182. Springer, Berlin (2015)
15. Iijima, T.: Basic theory on normalization of pattern (in case of typical one-dimensional pattern). *Bulletin of the Electrotechnical Laboratory* **26**, 368–388 (1962), in Japanese
16. Iske, A.: *Multiresolution Methods in Scattered Data Modelling*, Lecture Notes in Computational Science and Engineering, vol. 37. Springer, Berlin (2004)
17. Kozhokin, N., Savchenko, V., Senin, M., Hagiwara, I.: An approach to surface retouching and mesh smoothing. *The Visual Computer* **19**(8), 549–564 (2003)
18. Lehmann, T., Gönner, C., Spitzer, K.: Survey: Interpolation methods in medical image processing. *IEEE Transactions on Medical Imaging* **18**(11), 1049–1075 (1999)
19. Madych, W.R., Nelson, S.A.: Polyharmonic cardinal splines. *Journal of Approximation Theory* **60**(2), 141–156 (Feb 1990)
20. Mainberger, M., Bruhn, A., Weickert, J., Forchhammer, S.: Edge-based image compression of cartoon-like images with homogeneous diffusion. *Pattern Recognition* **44**(9), 1859–1873 (Sep 2011)
21. Mainberger, M., Hoffmann, S., Weickert, J., Tang, C.H., Johannsen, D., Neumann, F., Doerr, B.: Optimising spatial and tonal data for homogeneous diffusion inpainting. In: Bruckstein, A., Haar Romeny, ter, B., Bronstein, A., Bronstein, M. (eds.) *Scale Space and Variational Methods in Computer Vision*, Lecture Notes in Computer Science, vol. 6667, pp. 26–37. Springer, Berlin (Jun 2012)
22. Masnou, S., Morel, J.: Level lines based disocclusion. In: *Proc. 1998 IEEE International Conference on Image Processing*. vol. 3, pp. 259–263. Chicago, IL (Oct 1998)
23. Peter, P., Hoffmann, S., Nedwed, F., Hoeltgen, L., Weickert, J.: Evaluating the true potential of diffusion-based inpainting in a compression context. *Signal Processing: Image Communication* **46**, 40–53 (Aug 2016)
24. Schmaltz, C., Peter, P., Mainberger, M., Ebel, F., Weickert, J., Bruhn, A.: Understanding, optimising, and extending data compression with anisotropic diffusion. *International Journal of Computer Vision* **108**(3), 222–240 (Jul 2014)
25. Schmidt, M., Weickert, J.: Morphological counterparts of linear shift-invariant scale-spaces. *Journal of Mathematical Imaging and Vision* **56**(2), 352–366 (2016)
26. Schönlieb, C.B.: *Partial Differential Equation Methods for Image Inpainting*. Cambridge University Press, Cambridge, UK (2015)
27. Stein, M.L.: *Interpolation of Spatial Data – Some Theory for Kriging*. Springer, New York, NY (1999)
28. Uhlir, K., Skala, V.: Radial basis function use for the restoration of damaged images. In: Wojciechowski, K., Smolka, B., Palus, H., Kozera, R., Skarbek, W., Noakes, L. (eds.) *Computer Vision and Graphics, Computational Imaging and Vision*, vol. 32, pp. 839–844. Springer, Dordrecht, Netherlands (2006)
29. Wendland, H.: *Scattered Data Approximation*. Cambridge University Press, Cambridge, UK (2005)

30. Yuille, A.L., Grzywacz, N.M.: A computational theory for the perception of coherent visual motion. *Nature* **333**, 71–74 (1988)